Modification of an Operational Dispersion Model for Urban Applications

PETER DE HAAN,* MATHIAS W. ROTACH, AND MAJA WERFELI

Swiss Federal Institute of Technology, Institute for Climate Research, Zurich, Switzerland

(Manuscript received 21 December 1999, in final form 6 September 2000)

ABSTRACT

An operational multisource, multireceptor Gaussian dispersion model, the Danish regulatory model Operationelle Meteorologiske Luftkvalitetsmodeller (OML) has been modified for applications in urban environments. A so-called roughness sublayer has been introduced into the model to represent the turbulence characteristics of the lowest part of the surface layer over rough surfaces like cities. The meteorological preprocessor was enhanced to take into account an urban energy budget. The performance of the resulting OML-Urban has been validated for nitrogen oxides and sulfur dioxide for Zurich for 1990. For that year, a detailed emission inventory as well as continuous hourly measurements at four stations are available. The 24 air pollution monitoring stations used for validation have been divided into different groups, depending on local influences from nearby roads. In comparison with results from the standard OML using an urban roughness length, the urban modification (roughness sublayer and changes in the meteorological preprocessor) results in a 25%–35% increase of the annual mean surface concentration. OML-Urban shows a good reproduction of the probability density function of observed hourly concentrations, and the simulated yearly averaged concentrations show a good correspondence to observations.

1. Introduction

Air pollution modeling in urban areas is different from the traditional single high-stack source dispersion problem in several ways. The air pollution level in agglomerations often is dominated by a countless number of small, not-well-determined emission sources. The inhomogeneity of the built-up area often causes concentration measurements to be locally influenced. Almost all emission sources are situated within the lowest tens of meters, where human living takes place, also.

Although crucial to microscale dispersion modeling, relatively little is known concerning the flow and turbulence structure over built-up areas. Irregularly spaced tall roughness elements such as buildings induce a roughness sublayer (RS), which ranges from ground level to several times the average building height (Raupach et al. 1991), as displayed in Fig. 1. The existence of a roughness sublayer is not specific to urban surfaces but, unlike the case of smoother terrain, its vertical extension cannot be neglected. Within this RS the flow and turbulence fields are different from that of the surface layer above (Högström et al. 1982; Rotach 1993a,b, 1997b; Roth and Oke 1993; Roth 1993; Oikawa and Meng 1995).

Gaussian plume models represent a valid (analytical) solution to the diffusion equation only for idealized circumstances. Stationarity and homogeneity of the turbulence characteristics are requested. In practice, none of these conditions is fully satisfied, but Gaussian plume dispersion models have been successfully used for rural configurations. Extensive validation has been done on tracer experiments conducted, for example, in Kincaid and Prairie Grass (e.g., Olesen 1995; Carruthers et al. 1992). Gaussian plume models have also been tested against tracer experiments in urban surroundings such as in the Indianapolis experiment (Hanna and Chang 1993). Especially for the prediction of yearly averaged concentration based on hourly meteorological data, Gaussian plume models are still the method of choice. Also, Gaussian plume dispersion models have been applied to multisource, multireceptor situations in inhomogeneous urban environments (e.g., Gryning and Lyck 1984; Härkönen et al. 1998).

This paper addresses the following changes that should be made to apply Gaussian plume models to urban environments:

1) changes to the computing code of the dispersion model and its meteorological preprocessor (to take into account the turbulence characteristics and the energy balance over urban surfaces),
2) changes in the setup of the model (emission height

* Current affiliation: INFRAS Ltd., Bern, Switzerland.

Corresponding author address: Peter de Haan, INFRAS Ltd., Muehlemattstr. 45, CH-3007 Bern, Switzerland.
E-mail: peter.dehaan@infras.ch

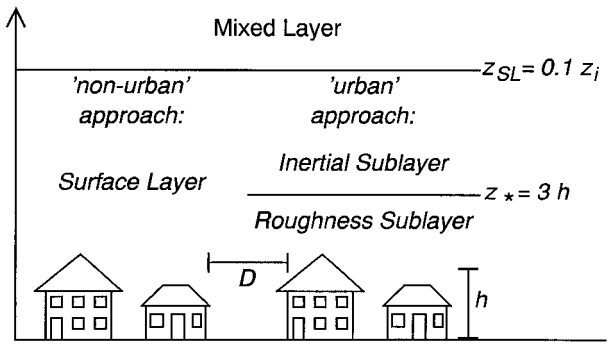

FIG. 1. Conceptual sketch of the lowest layers within the boundary layer over an urban surface. The left-hand side of the figure shows the situation as it is conventionally used in applied dispersion models (nonurban in the current terminology), and the right-hand side depicts the actual situation with a roughness sublayer adjacent to the surface (referred to as urban in the text). The height of the roughness sublayer is chosen as three times the average building height h for this study. Here, D denotes the average horizontal spacing of the roughness elements (see text for more details).

of sources and receptor heights within the urban canopy layer), and

3) changes in model validation by classifying measuring sites into different groups depending on the influence of nearby roads and building structures.

Rotach (1997a) proposed a method to introduce the RS into dispersion models by using an ''urban meteorological preprocessor.'' Because one of the main characteristics of an RS is the fact that the turbulent fluxes are not constant with height, the urban meteorological preprocessor allows for a nonconstant Reynolds stress in the RS. This nonconstant stress leads to higher wind speeds as compared with a logarithmic wind profile (Rotach 1993a), and the concept of local scaling is used to determine turbulence statistics such as velocity variances (Rotach 1993b). If the dispersion model uses similarity theory instead of stability classes, the concept of local scaling within the RS needs to be implemented in the dispersion model itself. The parameterizations of urban stability and the urban energy budget affect the meteorological preprocessor only.

The treatment of the RS after Rotach (1997a) proved to be successful in improving the performance of dispersion models. For a Lagrangian stochastic particle model, Rotach and de Haan (1997) showed that the underprediction of surface concentrations for the Copenhagen tracer experiment vanishes (Olesen 1995). De Haan et al. (1998) introduced the RS concept into an operational Gaussian dispersion model (which is much more suited to handle multisource, multireceptor problems), the Danish regulatory model Operationelle Meteorologiske Luftkvalitetsmodeller (OML) (cf. section 2a). A similar performance improvement for the Copenhagen and, in addition, for the Lillestrøm tracer dataset has been achieved.

This paper focuses on this modified version of the OML with an urban preprocessor, hereinafter called ''OML-Urban,'' which is applied to an entire city. The concept of the RS and other necessary changes to the OML meteorological preprocessor and dispersion model are presented (sections 2b and 2c). The resulting OML-Urban is validated using an extensive dataset from the city of Zurich. Measurements of nitrogen oxides (NO_x) and sulfur dioxide (SO_2) are available at 28 different sites, which are divided into groups with different characteristics (section 3). It is shown that the concept of the urban modification leads to a clear improvement of the predictions of the OML model. The resulting simulated annually averaged surface concentrations are in good agreement with measurements at 28 sites (section 4).

2. Adaptation of the OML dispersion model to urban conditions

a. OML dispersion model

The so-called OML is the basic atmospheric dispersion model for environmental impact assessments in Denmark. Besides the scientific multisource/multireceptor version used in the current work, OML-Multi, a single-source version for regulatory purposes is available (OML-Point). The OML is a Gaussian plume model, but, in contrast to many traditional regulatory models, its physical description is not based on the traditional discrete stability categories (Pasquill–Turner stability classes). Instead, the model uses basic boundary layer scaling parameters (see below).

The OML is intended to be used for distances of up to about 20 km from the source. It requires information on emissions and meteorological conditions on an hourly basis and returns a time series of concentrations calculated at user-specified receptor points. For a more detailed description of the model see Olesen et al. (1992). The lower boundary of the model domain in the vertical direction equals the roughness length z_0. Perfect reflection without deposition is assumed. This is done by placing a mirror source below the ground.

The meteorological preprocessor accompanying the OML is based on the resistance method (Berkowicz and Prahm 1982). The method used is one-dimensional, that is, neglecting heterogeneous surface conditions and topography. A description can be found in Olesen and Brown (1992).

b. Characteristics of the roughness sublayer

Within the RS, the flow and turbulence structure is different from that of the surface layer, which latter usually constitutes the lowest part of applied (operational) dispersion models. The most striking difference is the fact that the turbulent fluxes of momentum (and heat) are not constant with height (cf. the identification of the surface layer as a ''constant flux layer''): obser-

vations show an increase in momentum transport $\overline{u'w'}$ with height (Rotach 1993a; Oikawa and Meng 1995; Feigenwinter et al. 1999; Rafailidis 1997). Rotach (1993a) has presented a parameterization for the vertical profile of the local characteristic velocity (as derived from the Reynolds stress profile) within the roughness sublayer. However, this parameterization is highly site-specific and therefore is difficult to transfer to other applications. By taking into account the more recent full-scale observations of Oikawa and Meng (1995) and Feigenwinter et al. (1999), a more general parameterization can be found:

$$\left[\frac{u_{*,l}(z)}{u_*^{\mathrm{IS}}}\right]^b = \sin\left(\frac{\pi}{2}Z\right)^a \qquad (Z \le 1), \tag{1}$$

where $u_{*,l}(z)$ is the local friction velocity, $u_{*,l}(z) = [-\overline{u'w'}(z)]^{1/2}$, and u_*^{IS} is the friction velocity as derived from Reynolds stress at the upper boundary of the roughness sublayer, $z = z_*$. Further, $Z = z'/z'_*$ is a nondimensional height using $z' = z - d$ and $z'_* = z_* - d$, where d is the zero-plane displacement. The parameters a and b are fitted to the data of the three full-scale data sets, yielding $a = 1.28$ and $b = 3.0$. More detail on this parameterization can be found in a recently submitted paper (Rotach 2001).

The nonconstant Reynolds stress within the RS leads to a smaller gradient of mean wind speed as compared with the ''logarithmic profile'' of the surface layer (Rotach 1993a) and the necessity to revise the scaling concept for the turbulence statistics such as velocity variances (Rotach 1993b; Roth 2000). Instead of using a constant value of the friction velocity to scale velocity variances within the RS, Rotach (1993b) uses local scaling with the height-dependent scaling velocity.

Both of these features are likely to modify dispersion characteristics and hence surface concentrations over urban surfaces, and this modification may be severe because of the relatively large vertical extension of an urban RS. Within the meteorological preprocessor, for all observed friction velocity values from measurements within the RS, a ''reference'' friction velocity u_*^{IS} that is representative for the inertial sublayer (IS) is computed according to Eq. (1). In the dispersion model, velocity variances are scaled with u_*^{IS} in the IS. In the RS below, a height dependent local characteristic velocity $u_{*,l}(z)$ is used. The same local scaling approach applies to the mean wind speed profile within the RS.

c. Introduction of an urban energy balance into the meteorological preprocessor

This section describes the modification of the original OML meteorological preprocessor (Berkowicz et al. 1985) to take into account an urban energy budget. Meteorological preprocessing often relies on parameterizations based on measurements in rural environments. The main differences among rural, vegetated surfaces, and surfaces of cities are a reduced evaporation, because of the fast runoff and built-up areas, and a limited storage capacity for water. Therefore cities have a smaller latent heat flux. Furthermore, the roughness is much higher as compared with rural surfaces, often comparable to the roughness of forests.

The standard OML meteorological preprocessor computes turbulence parameters (heat flux, friction velocity, Obukhov length, net radiation) using the resistance method of Berkowicz and Prahm (1982). This method assumes analogy with Ohm's law to parameterize the resistance of the surface to evaporation and the flux of heat and water vapor through the surface layer. Berkowicz and Prahm (1982) determine the parameters needed to describe the stomatal resistance from data for three types of grass vegetation only. Lack of appropriate data disables the use of the resistance method for urban situations. Therefore OML–Urban computes the surface fluxes of heat H and latent heat λE using the scheme of Holtslag and van Ulden (1983). Their scheme, following the Penman–Monteith approach (Monteith 1981), also depends on two empirical parameters α and β'; the sensible heat flux is parameterized as

$$H = \frac{(1 - \alpha) + \gamma/s}{1 + \gamma/s}(Q^* - G) - \alpha\beta' \tag{2}$$

and the latent heat flux as

$$\lambda E = \alpha\left[\frac{1}{1 + \gamma/s}(Q^* - G) + \beta'\right], \tag{3}$$

where Q^* denotes the net radiation, G is the ground heat flux, $s = \partial q_s/\partial T$, q_s is the saturation specific humidity, $\gamma = C_p/\lambda$, C_p is the specific heat of air at constant pressure, and λ is the latent heat of water vaporization.

In urban environments, H is often found to be positive (although small) during nighttime. This result is due to the storage fluxes, which play an important role in the urban energy balance. The storage fluxes transfer daytime energy into nighttime, producing higher minimum temperatures during nighttime. For the change of the storage flux, a parameterization after Arnfield and Grimmond (1998) is used,

$$\Delta Q_s = a_1 Q_* + a_2\frac{\partial Q_*}{\partial t} + a_3 \tag{4}$$

where $\partial Q_*/\partial t = (Q_{*t-1} - Q_{*t+1})/2$, $a_1 = 0.41$, and $a_2 = 0.05$ h. We have chosen $a_3 = -43.67$ W m^{-2} instead of the -40 W m^{-2} proposed by Arnfield and Grimmond (1998) in order to have on average (over 12 months) $\overline{\Delta Q_s} = 0$. The anthropogenic heat flux Q_F is a function of the hour of the day, $Q_F(\mathrm{hour}) = \overline{Q_F}\{1 - 0.6\cos[\pi(\mathrm{hour} - 3)/12]\}$. Here, $\overline{Q_F} = 62.5$ W m^{-2} in January, $\overline{Q_F} = 37.5$ W m^{-2} in July, and it is linearly extrapolated in between. So, for each hour, $Q_* + Q_F = \Delta Q_s + \lambda E + G + H$.

The value of α can be computed from observations;

it depends on the surface moisture condition. For bare soil, $\alpha = 0$, so that $\lambda E = 0$. For the Prairie Grass experiment, $\alpha = 0.45$ (Holtslag and van Ulden 1983). For vegetated surfaces with enough water to evaporate, $\alpha = 1$. Because of the reduced water storage capacity and the fast runoff, the following parameterization has been introduced into OML's preprocessor for use over urban surfaces:

$$\alpha = \begin{cases} 1 & \text{hours with rain reported} \\ 0.45 & \text{accumulated net radiation} < 300 \text{ W h m}^{-2} \\ 0.2 & \text{otherwise.} \end{cases} \tag{5}$$

The accumulated net radiation is calculated as the sum of the net radiation for each hour since rainfall stopped. With Eq. (5), the parameter α is not a constant anymore, and the urban energy budget becomes a function of the accumulated net radiation.

The net radiation Q^* is calculated with OML's routine, which is based on the scheme of Nielsen et al. (1981). For daytime hours, this scheme calculates Q^* as a function of the global radiation, the albedo, and the cloud cover. Hourly values of global radiation are available from a station of the Swiss National Weather Service located within Zurich. For nighttime hours, Q^* is computed using the nighttime formula of Nielsen et al. (1981), which is based on regression analysis of measured data. Transition of night- to daytime hours and vice versa is defined by the sign change of the solar elevation angle.

The albedo is set to 0.16 for nonsnow surfaces (Oke 1988). For snow-covered surfaces, albedo values found in the literature range from 0.95 for fresh snow to 0.40 for old snow (Stull 1998, p. 258). In this study, 0.60 has been chosen as averaged snow albedo value, reflecting the fact that, within cities, the snow normally is removed from major streets immediately and gets dirty soon. The saturation water vapor pressure of moist air, needed to compute s, is computed after a scheme of Buck (1981). The ground heat flux G is parameterized as a function of the net radiation. We use the following expression derived by Oke and Cleugh (1987) for a suburban area:

$$G = \begin{cases} 0.35(Q^* - 27 \text{ W m}^{-2}) & \text{(daytime)} \\ 0.75Q^* & \text{(nighttime)} \end{cases} \tag{6}$$

In Eq. (6), we changed the original daytime coefficient of 0.25 to 0.35 because the Oke and Cleugh (1987) formula applies to suburban rather than urban environments. For the same reason, the original nighttime coefficient of 0.67 has been increased to 0.75. These new coefficients are somewhat below those given by Arnfield and Grimmond (1998) for an urban street canyon.

Irregularly spaced, large roughness elements affect the stability regime. Such elements cause additional mechanical turbulence. This turbulence leads to a tendency for the atmospheric nighttime stability toward neutral conditions, when compared with the rural areas surrounding the city. During daytime, the same roughness elements counteract the development of large convective eddies as well as a pronounced negative potential temperature gradient. This result causes a trend of the daytime stability regime toward neutral conditions also.

The default minimum value of the Obukhov length within the standard version of the OML preprocessor is $100z_0$, that is, roughly equal to 10 times the average obstacle height. For cities, the roughness length typically is estimated at 1 m. This value would imply a minimum Monin–Obukhov length L value of 100 m. Hanna and Chang (1992, 1993) use minimum L values over urban terrain that are a function of the height of the roughness elements h. Their parameterization corresponds to a $75z_0$ limit. We adopt this limit for OML-Urban. We apply the minimum value to unstable atmospheric stability as well, that is,

$$|L|_{\min} = 75z_0. \tag{7}$$

The minimum value of the friction velocity, which has an original minimum value of 0.001 m s^{-1} within the standard OML, has been raised to $u_{*,\min} = 0.01$ m s^{-1} in OML-Urban. This value reflects the increased production of mechanical turbulence within cities and is in accordance with Eq. (7).

d. Modification of the dispersion model

Apart from the local scaling with the friction velocity (presented in section 2b), further changes to OML are needed for urban applications. Within cities, almost all emissions originate from combustion processes (road traffic, domestic heating, waste incineration, etc.) and thus have a buoyancy- and momentum-induced plume rise. For gridded emission inventories, instead of individual stack characteristics (diameter, temperature excess, and vertical exit velocity), representative buoyancy and momentum fluxes are to be estimated.

OML uses the plume rise schemes of Briggs (1984) for point sources. OML-Urban has been enhanced to account also for the buoyant rise of area sources. The main parameters to determine final rise height of the buoyant release are the buoyancy flux, the mean wind speed at the stack tip, and the friction velocity. For OML-Urban, characteristic emission heights are chosen for domestic heatings and traffic area sources. Rather than vertical exit velocity and source radius, averaged buoyancy fluxes are assigned to the area sources depending on the source strength. The emission temperature is assumed to be constant (rather than assuming a constant temperature excess with respect to the ambient temperature). This assumption reflects the more or less constant operation temperature of engine vehicles and of heating installations.

The well-known Gaussian plume solution to atmospheric dispersion does not apply close to the source,

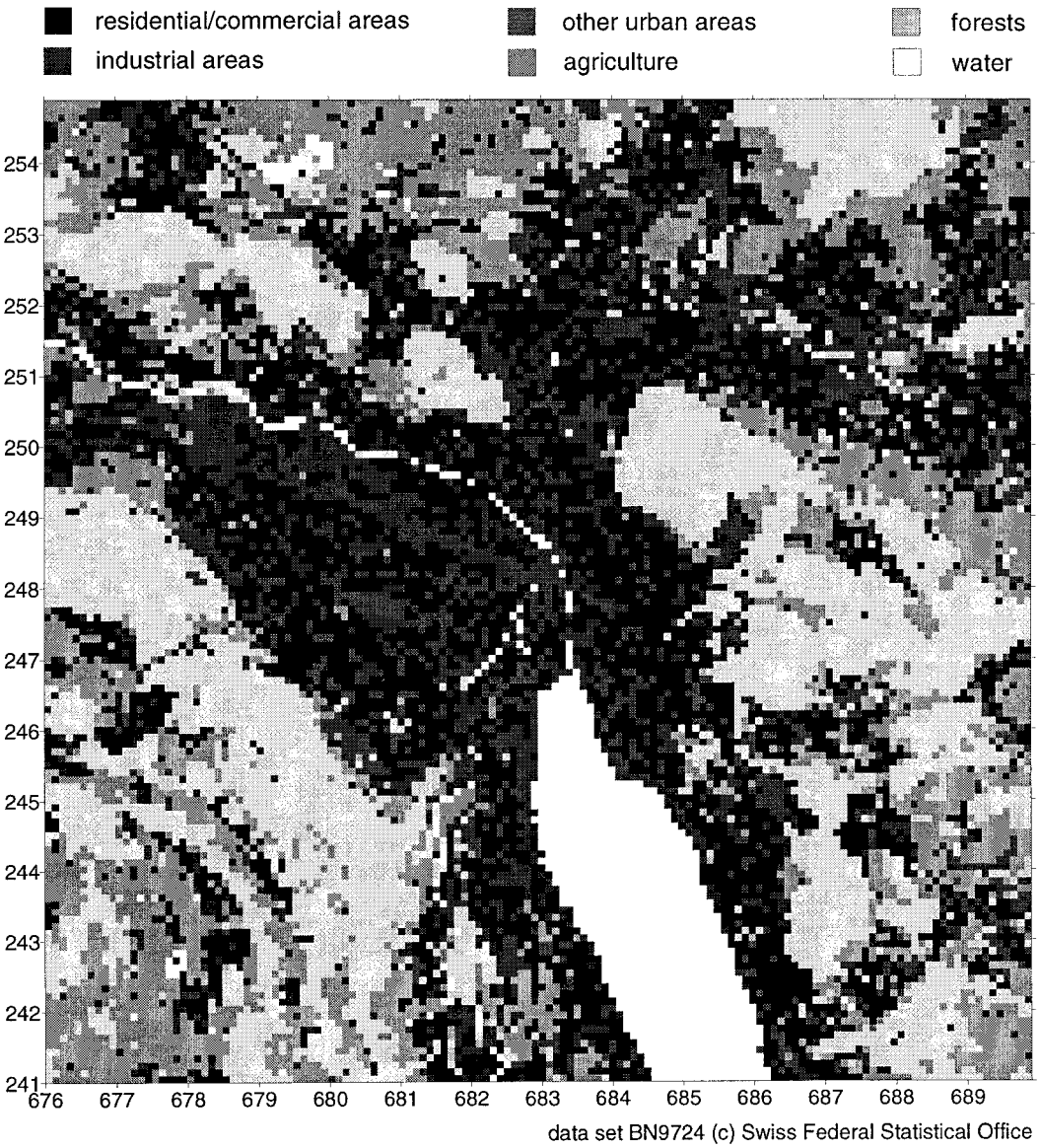

FIG. 2. Land use (100 m × 100 m resolution; south–north and east–west axes use the Swiss coordinate system with 1-km spacing) of the city of Zurich and its surroundings, aggregated into six main categories. The city center is roughly situated at the transition of the Lake of Zurich (southern part of the figure) to the Limmat River.

because all parameterizations of the vertical and lateral plume standard deviations $\sigma_y(x)$ and $\sigma_z(x)$, respectively, approach zero near the source. This fact causes the ground-level concentration prediction of Gaussian plume models to approach infinity for $x \to 0$. Therefore, in the OML, first $\sigma_y(x)$ and $\sigma_z(x)$ are computed at a certain minimum distance from the center of the area source to handle the situation where a receptor is placed inside an area source. Second, a lower limit applies to $\sigma_y(x)$ and $\sigma_z(x)$. The combined effect can be expressed as $\sigma_i(x) = \max\{0.5\Delta x, \sigma_i[\max(0.5\Delta x, x)]\}$, where Δx denotes the horizontal extension of the area source, and $i = y, z$.

3. Zurich 1990 case study

a. Zurich 1990

The city of Zurich has approx. 370 000 inhabitants and covers an area of 88 km^2. This area consists of 4226 ha of natural surface (forests, parks, agricultural areas, cemeteries, and water) and 4548 ha of covered surface (buildings, roads, infrastructure, and industry). Figure 2 depicts the land use of Zurich aggregated into six main categories.

Data are available from a meteorological station that is situated within the city (shown in Fig. 4). The station is situated at the headquarters of the Swiss National

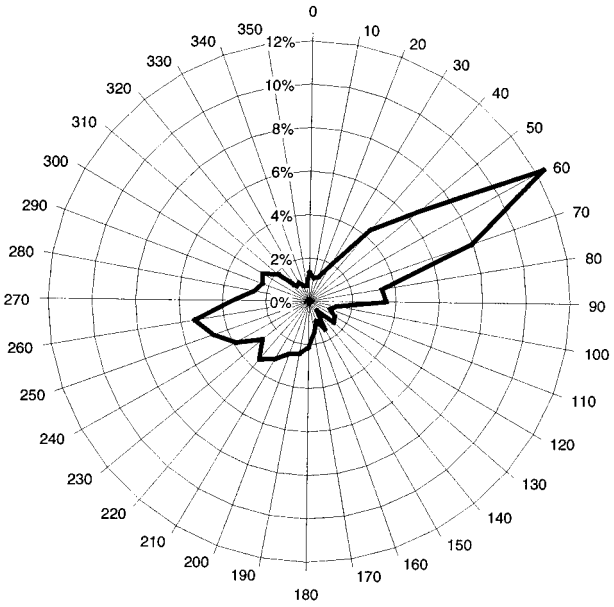

FIG. 3. Wind rose of all hours of observed wind direction for 1990 at the meteorological station of the Swiss Meteorological Service in Zurich.

Weather Service, in a residential area, surrounded by buildings with 2–3 stories. This station covers all ground observations needed. As an example, the wind rose for the entire year of 1990 is depicted in Fig. 3. For the determination of the mixing height, the OML preprocessor requires vertical profiles of temperature and density. We use the upper-air soundings (twice daily) from the Payerne station, the most nearby upper-air station, 200 km away from Zurich in a SWW direction. Payerne and Zurich are both located in the so-called Swiss Central Plateau, which denotes the densely populated area between the Jura and the Alps mountain ridges. These mountain ridges cause some channeling, as can be seen in Fig. 3.

b. Classification of concentration measurement locations

For 1990 we have surface concentration data from 28 stations. Figure 4 shows their locations. Four stations monitored continuously (hourly averages) during the whole year. At the remaining 24 stations, the annual concentration is estimated from 40 to 45 measurements of 24 h each (covering all seasons and all days of the week).

The use of gridded emission inventories limits us to the prediction of area-averaged concentrations. The measurements essentially are point concentrations. These point concentrations may be influenced by local emission sources (such as major roads), or they may not be (yielding the urban background concentration). If local influences are present, they may either be resolved by the emission inventory or they may not be. We therefore validate the model performance separately for three groups, as defined in Table 1 (''urban background,'' ''partly influenced by major roads,'' and ''dominant local influences''). To determine the specific group, all measurement sites have been investigated in detail. The environment of each measurement site is classified according to Table 2. The immediate and local environment of each measurement site were assessed using maps. Some locations also were visited in the field. Table 3 describes the concentration monitoring sites, along with the coordinates as depicted in Fig. 4. The boundary for the ''immediate'' environment has been set to 100 m, that of the ''local'' environment to 1 km. For stations situated near major roads, the daily traffic volume also is given. The resulting station classifications in the groups Q1, Q2, and Q3, respectively, are listed in Table 3. The immediate environment is the most dominant. Any dispersion model would be expected to perform best in predicting the urban background (Q1 data in this study) and second best in predicting concentrations where roads are adequately resolved in the emission inventory (Q2) and to show considerable error when local effects are present on scales smaller than the spatial concentration sampling scale (Q3).

c. Emission inventory

Estimating the total emissions of an agglomeration is difficult. Uncertainties exist on the emission factor of road traffic as well as the traffic volume itself, on the emission factors for the various other fossil burning processes, and so on. No dispersion model prediction can be more accurate than the emission inventory it relies upon. We do not address these inherent uncertainties of urban emission inventories here.

For Zurich in 1990, a detailed (100 m $\times$ 100 m resolution) emission inventory was constructed (Werfeli 1995). It takes into account traffic (number of vehicles per day and estimated speed on the 152 largest roads of the city and estimates of short-distance traffic not using major roads), domestic and commercial heating, and the 33 largest industrial sources (treated as point sources in the model).

This emission inventory sums up to over 4300 SO_2 sources and over 4300 NO_x sources, where the line sources (roads) are split up and added to area sources. To simulate the time dependence of source strength, the amplitude of the traffic sources is modulated according to the hour of the day and the day of the week, and the strength of the heating sources depends on the hour of the day and on the month. Among the observational data, traffic volume data at four sites within the city are available and have been used to construct average hourly and daily frequency cycles.

The emission data of the heating sources were collected very carefully, and the traffic emissions were modeled using numerous results from actual traffic census data. The emission factors used for the calculation

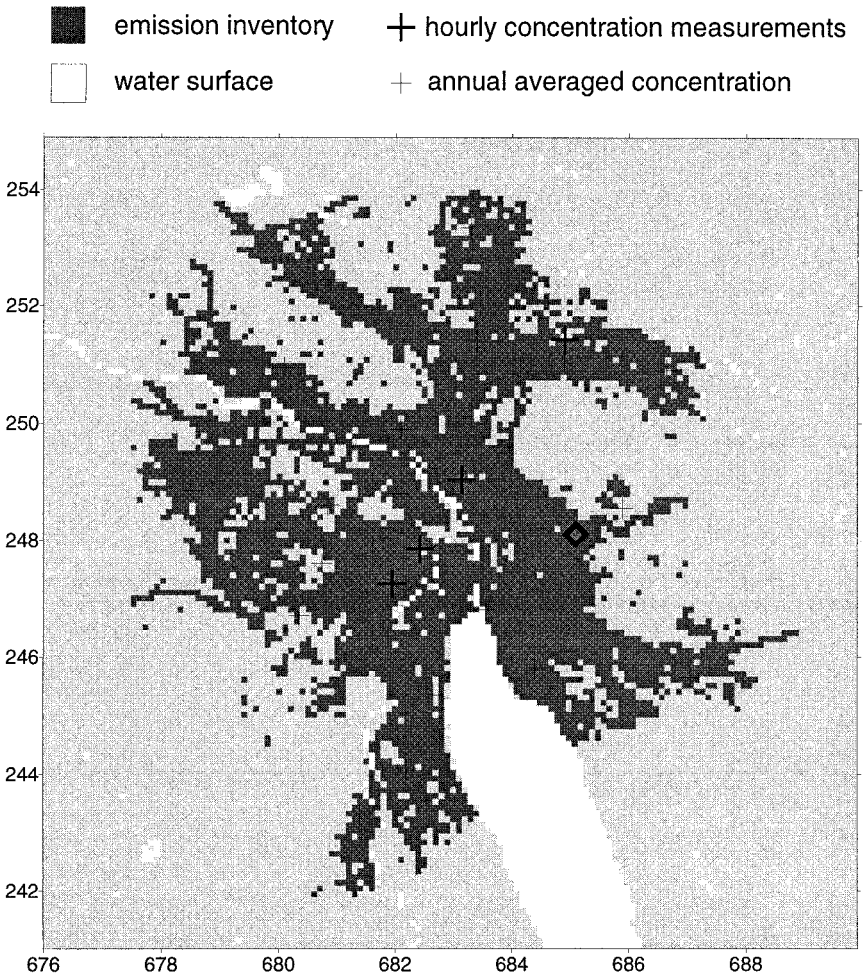

FIG. 4. Location of air pollution monitoring stations and spatial extension of the emission inventory with 100 m × 100 m resolution (for 1990). The location of the National Weather Service meteorological station is denoted by "◇."

of the overall emissions for each source type and pollutant were checked with on-site monitoring measurements. With this procedure, the overall accuracy of the total citywide emission is estimated at ±5% for heating sources (SO_2 and NO_x) and at ±20% for NO_x and ±25% for SO_2 for emissions from traffic sources. This amounts to a total maximum estimated error in the emission data of 6.3% for SO_2 and, because of the larger contribution of traffic sources, 14.3% for NO_x.

d. Urban setup

The definition of the model surface is a key factor in urban dispersion modeling. In urban environments, there is no such thing as an averaged mean wind speed in the lowest, say, 10 m, that is, between the building structures themselves. To avoid the use of a (relatively simple) Gaussian model for dispersion estimates *between* the roughness elements, a model surface corresponding to the zero displacement height (see Rotach 1994) rather than the physical surface ($z = 0$) has been chosen. Oke (1988, p. 472) also suggests that the effective surface lies at about the level of the sum of the zero-plane displacement and roughness height. For Zurich, the average building height is $h = 12$ m; the thickness of the RS has been chosen to be $3h$. This approach corresponds to the one adopted by Hanna and Chang

TABLE 1. Definition of concentration measurement station groups in urban areas.

Group	Description	Examples of locations
Q1	True urban background concentration	Park areas within city, residential areas with very low traffic
Q2	Urban background concentration with local influences	Residential areas with nonmajor roads
Q3	Street concentration station	Street canyon, near major roads

TABLE 2. Description of immediate and local environment of air pollution monitoring stations according to European Union Council Directive 92/72/EC on Air Pollution by Ozone.

Immediate Environment (within a radius of 0 to 100 m)	
I1a, I1b, I1c, I1d	Large street heavy/medium/local/ no traffic
I2a, I2b, I2c, I2d	Small street heavy/medium/local/ no traffic
I3a, I3b, I3c, I3d	Canyon street heavy/medium/local/ no traffic
I4	Footway
I5	Front of building
I6	Terrace, tower, belfry
I7	Interior court, school, hospital
I8	Trees
I9	Large flat area
I91	Channel
I92	Meadow, field
I99	Other
Local Environment (within a radius of 100 m to some kilometers)	
LAa, LAb, LAc, LAd	Urban commercial/industrial/residential/mixed
LBa, LBb, LBc	Industrial heavy/medium/light concentration
LCa, LCb, LCc	Road traffic heavy/medium/ light
LD	Commercial
LE	Residential (isolated houses)
LF	Harbor
LG	Airport
LH	Park, forest, natural field
LI	Agricultural area
LJ	Mountains, valleys
LK	Sea side or lake side
LL	Other

(1993), in which the depth of the mechanically well-mixed layer is set at three times the average obstacle height.

The zero displacement height is set at $d = 0.75h$ (Rotach 1994), as sketched in Fig. 5. The height of the domestic and industrial area sources has been set to 5 m above the average building height, reflecting the fact that chimneys are situated at the very top of every building and that, in general, high buildings have stacks with high emission rates. The emission height of the traffic area sources corresponds to the lower model boundary. For the 33 largest sources, which are treated as individual point sources within this simulation, the emissions take place at the physical stack height. All concentrations have been predicted for a receptor height of $z' = 0$ m, where $z' = z - d$, that is, at the lower model boundary.

No attempt has been made to develop vertical profiles of concentration within street canyons to extrapolate any concentrations predicted at the $z' = 0$ m level down to the physical ground level. In general, concentrations at street level are higher than at a height of several meters, that is, $z' = 0$ m (e.g., Lee and Park 1994; Zoumakis 1995). The measurements were taken at 2 m above ground level, that is, well below $z' = 0$ m (for some of the continuously measuring stations, the receptor height is 5 m). But because the emission inventory does not resolve single street canyons and because such influences depend on the wind direction and the surrounding buildings, such an extrapolation cannot be expected to improve the model accuracy. Instead, we will (in section 4) evaluate the predicted concentrations for the stations groups Q1 to Q3 separately. It is assumed that street canyon effects only occur at Q3 sites.

Special care has been taken to estimate the buoyant plume rise of the emissions. The buoyancy flux, $F_B = gF_V\Delta T/T_a$, is determined by the estimated maximum volume flux (as summarized in Table 4) F_V caused by domestic heating. The maximum volume flux from Table 4 applies to daytime conditions during the coldest day of 1990 only. The actual volume flux is time dependent, where the same time series of scaling factors has been used as for the emission rate of the domestic area sources themselves (see preceding section). The temperature of the emission itself does not in general depend on the ambient temperature; it is determined by the technical layout of the heating equipment. Therefore a constant level of exhaust gas temperature has been chosen.

The exhaust gases from mobile sources will experience a buoyancy-induced rise also. Here, we only address the overall rise of traffic area source emissions, not of individual vehicles. Given the fact that the efficiency for gasoline engines is less than 40%, a considerable amount of heat is released through the tail pipe. But the exact proportion of energy being radiated as heat, emitted through the tailpipe, or being used for chemical reactions in the catalytic converters, is unknown. In general, the exhaust gas temperature does depend on the previous minutes of driving behavior of the vehicle. In congested (stop and go) traffic conditions, the catalytic converter is likely not to reach the required temperature level, causing the emission level to increase drastically as compared with fluid traffic conditions. Nevertheless the resulting buoyancy of traffic area sources has been scaled with the time series of traffic volume (see preceding section).

e. Effect of surrounding suburbs

The emission inventory does not include the anthropogenic sources situated in the vicinity of the city (suburban sources). The (yearly averaged) concentration impact from these sources will be spatially varying, with lowest values in the center of the domain, increasing toward the boundaries of the inventory.

This concentration map induced by suburban sources is obtained from another dispersion model estimating yearly averaged nitrogen dioxide (NO_2) concentrations for the whole of Switzerland (SAEFL 1997). For this study, a special concentration map has been computed based on the emission inventory of the state of Zurich, where all those sources that are situated within the capital city itself have been removed. This yields the

TABLE 3. Characteristics and classification of concentration measurement stations in the Zurich 1990 field campaign. Station type ''hourly conc.'' denotes continuous measurements, ''annual av.'' stands for statistically derived annual mean values. For definition of environment description, see Table 2. DTV denotes daily traffic volume (vehicles per day); ''Pop.'' is population density per hectare.

Station name	Type	*x* coordinate (km)	*y* coordinate (km)	Immediate environment (<100 m)	Local environment (<1 km)	DTV	Pop.	Noise level (dB*A*)	Group
Schwamendingen	Hourly conc.	684.91	251.43	I7	LAc, LCa		65	55	Q1
Schwamendingen 2	Annual av.	684.90	251.45	I7	LAc, LCa		65	55	Q1
Hard	Annual av.	680.85	248.60	I7	LAd		91	59	Q1
Seefeld	Annual av.	684.40	245.80	I7	LAc		91	60	Q1
Industriequartier	Annual av.	682.05	248.80	I7	LAd		134	52	Q1
Oberstrass	Annual av.	684.10	248.70	I7	LAc		64	57	Q1
Hirzenbach	Annual av.	686.65	250.90	I7	LAc, LCa		84	55	Q1
Sihlfeld	Annual av.	680.75	247.60	I8	LAc		—	52	Q1
Enge	Annual av.	682.65	245.35	I8, I9	LAc, LK		—	57	Q1
Zoo	Annual av.	685.90	248.55	I8, I9	LH		—	47	Q1
Kaserne	Hourly conc.	682.43	247.85	I2c, I7	LAd		—	—	Q2
Witikon	Annual av.	687.05	245.65	I2c	LE, LH		34	58	Q2
Höngg	Annual av.	680.10	250.95	I2c	LE, LH		41	57	Q2
Wollishofen	Annual av.	682.20	244.10	I2c	LAc, LCa		47	53	Q2
Leimbach	Annual av.	681.40	243.30	I2c	LE, LJ, LCa, LH		30	54	Q2
Altstetten	Annual av.	678.55	248.85	I2c	LAc, LH		48	49	Q2
Affoltern	Annual av.	680.90	252.45	I2c	LE, LH		37	60	Q2
Seebach	Annual av.	683.30	253.35	I2c	LAc, LCa		41	55	Q2
Stampfenbach	Hourly conc.	683.14	249.04	I1b, I5	LAd	10 000	84	72	Q3
Stampfenbach 2	Annual av.	683.15	249.00	I1b, I5	LAd	10 000	84	72	Q3
Wiedikon	Hourly conc.	681.95	247.25	I1a, I3a	LAd	33 000	126	72	Q3
Wiedikon 2	Annual av.	681.95	247.25	I1a, I3a	LAd	33 000	126	72	Q3
Bellevue	Annual av.	683.55	246.80	I1a	LAa, LK	60 000	38	74	Q3
Friesenberg	Annual av.	680.35	246.70	I1a	LE	14 000	42	68	Q3
Wipkingen	Annual av.	682.10	249.90	I1a, I3a	LAd	63 000	103	80	Q3
Schörli	Annual av.	684.90	251.10	I1a, I3a	LAc, LH	83 000	65	75	Q3
Oerlikon	Annual av.	683.40	251.40	I3a	LAd	18 000	62	70	Q3
Hirslanden	Annual av.	685.00	246.10	I3b, I1b	LAc	15 000	74	72	Q3

complementary concentration map to the current work. The SAEFL (1997) dispersion model is simple, and does not take into account the urban characteristics of the area. But the results are accurate enough to account for concentrations from anthropogenic sources outside the city.

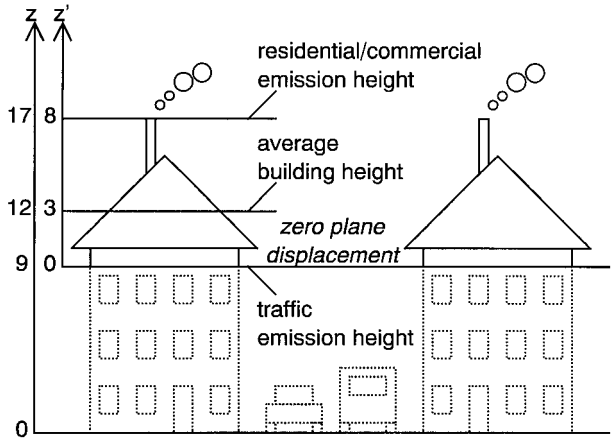

FIG. 5. Setup of the OML model for the Zurich simulation. Vertical axis gives height above ground in meters. The lower model boundary has been set to the zero-plane displacement height, which is set to three-quarters of the average building height. Traffic emissions are released at the bottom of the model domain. Receptor height for concentration prediction is $z' = 0$. For further explanations see text.

f. Background concentration

For the natural background concentration, a parameterization has been developed based on SAEFL (1997) that expresses the natural background as a function of the total nationwide emission load and altitude. For the latter, SAEFL (1997) derives an exponential decrease by fitting to observations. However, all regions in Switzerland below 650 m above mean sea level (MSL) are densely populated. A true background station at such

TABLE 4. Assumptions for the estimation of buoyant rise of area source (heating and traffic) emissions. The maximum buoyancy flux is multiplied with a monthly, daily, and hourly varying time series to obtain the appropriate buoyancy flux for each season (heating) or time of day (traffic).

	Domestic and commercial area sources	Traffic area sources
Max volume flux per household	18 m^3 h	
Avg No. of households per building	7.5	
Max volume flux per source	120 m^3 h^{-1}	2 m^3 h^{-1}
Absolute temperature of emissions	333.2 K	313.2 K

TABLE 5. Determination of NO_x-to-SO_2 ratio to derive the SO_2 from the NO_x background map. For each of the four stations with continuous measurements, the 10% (i.e., 876 h) of the hourly values with the lowest recorded concentration have been used.

Station	Station group	Mean of lowest 10% hourly concentration values		Ratio of NO_x to SO_2
		NO_x	SO_2	
Schwamendingen	Q1	22.1	1.2	18.7
Kaserne	Q2	20.8	1.7	12.1
Wiedikon	Q3	41.2	7.6	5.4
Stampfenbach	Q3	24.4	4.5	5.4

heights does not exist. For this study, all stations below 650 m MSL have been excluded, the result being that the natural background shows a linear rather than an exponential decrease as altitude increases. For 420 m MSL (representative of the city center of Zurich), the natural background then is 11 μg m^{-3} NO_x, as compared with the exceedingly high 30 μg m^{-3} in SAEFL (1997).

The NO_x total background concentration map consists of the natural background and the anthropogenic background from the suburbs (see preceding section). The SO_2 background map has been derived from the NO_x total background by a straightforward procedure. For the four stations with hourly observed concentration, the NO_x-to-SO_2 ratio of the average of the 876 h (i.e., 10% of the year) with the lowest observed concentrations has been computed (see Table 5). This ratio differs depending on the characteristics of the measurement station. For the true urban background (Q1 station), this ratio is higher as compared with the site with some local influences (Q2) and is much higher than for data obtained from sites exposed to streets (Q3). The SO_2 background concentration is derived by dividing the NO_x background concentration by 18.7, the ratio of the average of lowest 10% of NO_x measurements to the average of the lowest 10% of SO_2 measurements for the true urban background station.

Figure 6 depicts the resulting background maps. Using a fixed NO_x-to-SO_2 ratio for the whole domain means that we assume that the suburban sources of NO_x and SO_2 are spatially equally distributed. At the location where a major highway enters Zurich from the west, the resulting SO_2 background value might be overestimated (2.5 μg m^{-3} in the upper-left quarter of Fig. 6b), but none of the measurement sites used is located nearby.

4. Results

a. Overview

The OML has been used to predict SO_2 and NO_x concentrations at a uniform receptor height (located at the zero plane displacement height) at the positions of the 28 observational stations and at a regular grid covering the whole modeling domain with a spacing of 1000 m. The simulation has been run for the whole year of 1990, with a principal time step of 1 h.

Two different simulation runs have been conducted:

1) ''nonurban'' simulation, that is, application of the OML model ''as is,'' with the setup as shown in Fig. 5, roughness length $z_0 = 1$ m, and area source plume rise settings as outlined in section 3d; and
2) ''urban'' simulation, that is, application of the OML-Urban model, or the OML with the modifications

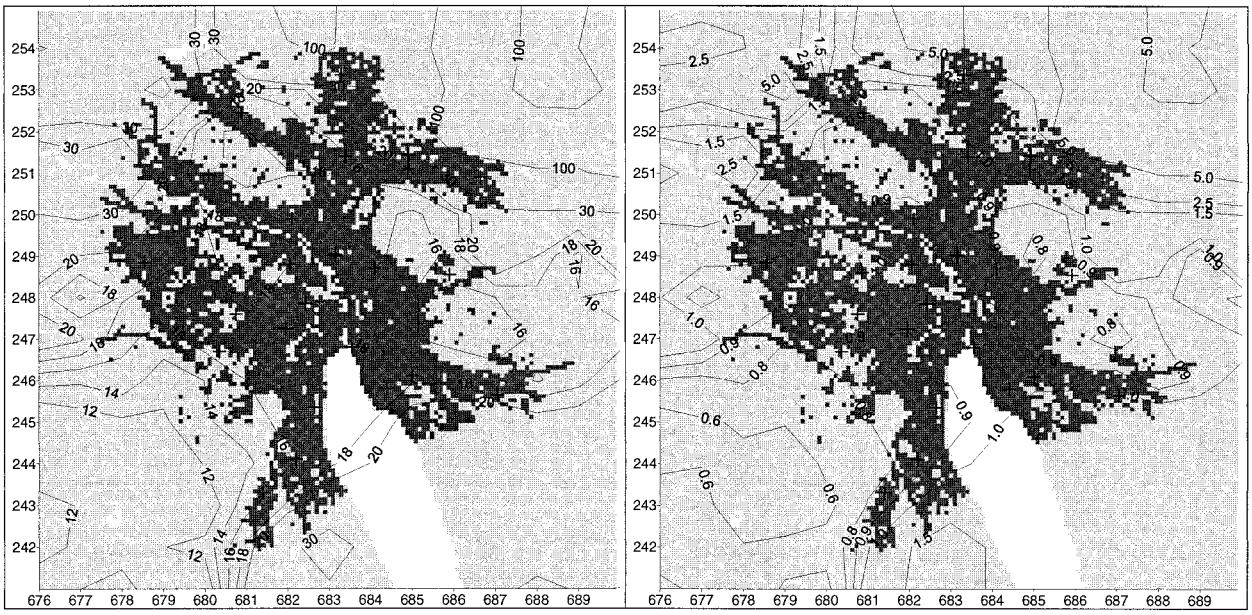

FIG. 6. Background concentration maps (the sum of the natural background concentration and the impact of all emission sources outside of the emission inventory domain) for (left) NO_x and (right) SO_2 for 1990. Annual averaged concentration: μg m^{-3}.

from section 2c [urban energy balance in meteorological preprocessor, Eqs. (2)–(7)] and section 2b (local scaling with friction velocity as a function of height); all other settings are identical to the nonurban simulation run.

The major goal of the investigation is the correct prediction of the annual average concentration. New-generation Gaussian plume models are generally accepted to be suited for such predictions. However, a wide range of assumptions regarding source characteristics inevitably has to be made, as has been outlined in the previous sections. To minimize the risk that the correct annual average prediction (as it can be verified with respect to the 28 observational stations) actually arises from the sum of various severe over- and underpredictions caused by inadequate parameterizations and/or source specifications, a multistep validation procedure is used [note that a validation of the standard version of the OML can be found in Olesen (1995), including several residual analyses.]

First, we will assess the effect of those parameters for which actual urban values have been chosen. Second, we will compare the hourly predicted concentration time series with the observed daily cycles of continuous (i.e., hourly) observations. Third, using quantile–quantile plots, it can be verified whether the distribution of predicted concentrations resembles the observed distribution. This procedure is done for the 8760 h of observations at the four continuously measuring stations. Last, we will calculate the performance statistics of the predicted annual mean concentration at the positions of the 28 observational stations, separately for each receptor ''station group.''

b. Pollutants considered

NO_2 frequently exceeds the threshold value of the Swiss clean air act. The permitted yearly average is 30 μg m^{-3} for NO_2; the threshold of 80 μg NO_2 m^{-3} may be exceeded only once per year based on a 24-h average, and the threshold of 100 μg NO_2 m^{-3} must not be exceeded during 95% of all 30-min averages over the whole year. These limits are considerably lower than in most other countries, including the United States. The chemical conversion of stack and tailpipe nitric oxide (NO) emissions to NO_2 takes place over distances of some hundreds of meters. Therefore, in this study, NO_x rather than NO_2 is modeled, because it is a more robust quantity.

On the side of the emission inventory, the NO_x emissions consist of the sum of the two components NO and NO_2. On the side of the measurements from the air pollution monitoring stations, again the sum of NO and NO_2 is used for NO_x. The assumption that NO_x can be assumed as a tracer quantity holds to a high degree.

The current study also models SO_2. Because of a general tendency of decreasing emissions, the importance of this pollutant as a risk factor to human health is decreasing. The corresponding annual average threshold (30 μg m^{-3}) of the Swiss clean air act is not violated anymore in Zurich at present. This fact is mainly due to the use of low-sulfur oil for domestic and commercial heating purposes. Also, the 100 μg m^{-3} threshold, which may be exceeded during only 1 day per year and during only 5% of all 30-min averages as well, is not violated any more at present. SO_2 has been included in this study because, unlike NO_x, which is emitted mainly by road traffic at street level, SO_2 originates for the larger part from residential and commercial nonmobile sources with different source characteristics.

c. Main effects of urban modification

In this section, we investigate the effect of the most important urban settings. Both the energy transfer from Eq. (4) and the increased mechanical mixing as introduced by Eq. (7) affect the stability regime. Table 6 compares the effect of these two parameterizations on H and L. As can be seen, the increased G and λE lead to more neutral conditions (higher number of hours with larger absolute value of L). The storage term of Eq. (4) leads to an additional shift toward more neutral conditions (rightmost column in Table 6). The effect of Eq. (4) is also clearly visible for the sensible heat flux, for which a pronounced shift toward small but nonnegative values can be observed. This result directly leads to a shift in the ratio of stable to unstable atmospheric stability, because the sign of the Obukhov length is ruled by the sign of the sensible heat flux. As a result, where the standard nonurban preprocessor predicts 63% stable hours (31% unstable), OML-Urban predicts the more realistic amount of 36% stable (57% unstable) for urban environments.

The roughness length z_0 has a pronounced influence because of the lower limit on the absolute value of L (Eq. 7). For the meteorological conditions of this study, 21% of all hours of the year are set to the stable limit ($L = 75z_0$) and 32% to the corresponding unstable limit of $-75z_0$. Note that this limit also is part of the standard OML meteorological preprocessor. The impact on the meteorological scaling parameters by the increased lower limit to the friction velocity adopted in this study (section 2b) is minor. Only for 39 h of the whole year, the friction velocity was increased to the minimum value of 0.01 m s^{-1}.

The simulation for Zurich for 1990, for which the results are discussed in the next sections, has also been performed with a ''semiurban'' approach, that is, by introducing the RS turbulence but without the urban modifications to the energy balance as discussed in section 2c (affecting the albedo, the snow albedo, the ratio of sensible to latent heat flux, and the moisture availability). The combined effect of these urban energy balance settings alone is a decrease in NO_x annual-averaged concentrations of 0.17% and a decrease of 1.8% for SO_2.

TABLE 6. Distribution of L and H for three different versions of the meteorological preprocessor. Nonurban stands for the standard OML preprocessor, with a roughness length of 1 m. "Urban, w/o Eq. (4)" denotes OML-Urban's preprocessor but without the storage term of Eq. (4). "Urban + Eq. (4)" gives the results for the full-scale OML-Urban preprocessor. For further explanations see text.

	Distribution of L				Distribution of H		
	Nonurban	Urban, w/o Eq. (4)	Urban + Eq. (4)		Nonurban	Urban, w/o Eq. (4)	Urban + Eq. (4)
<-5000	141	134	358	<-30	629	11	12
-5000 to -2000	106	96	269	-30 to -20	2062	904	114
-2000 to -500	255	233	544	-20 to -10	2624	2664	3079
-500 to -75.1	896	874	1365	-10 to -5	374	958	36
-75.1 to -74.9	1427	2101	2785	-5–0	247	785	198
-74.9–0	0	0	0	0–5	234	337	1374
0–74.9	0	0	0	5–10	173	115	716
74.9–75.1	3537	2819	1847	10–20	312	142	221
75.1–500	1124	1042	731	20–75	957	865	1080
500–2000	610	737	372	75–100	304	275	335
2000–5000	263	325	199	100–200	824	745	946
>5000	401	399	290	>200	20	959	649
Sum (h)	8760	8760	8760	Sum (h)	8760	8760	8760

Because the major part of domestic emissions (which dominate the SO_2 concentrations) is emitted during winter conditions, the larger effect on SO_2 concentrations is likely to be caused in large part by the change in snow albedo.

d. Hourly predictions: Reproduction of frequency distribution

Figure 7 shows an example of the hourly observed and predicted (both nonurban and urban approaches) NO_x concentrations. The daily cycle with concentration peaks induced by the road traffic peak hours can be clearly seen (the station depicted is a Q2 station with some influence from local traffic but not located directly near a road) as can the much lower concentration level on 16 September (a Sunday).

Gaussian models with gridded emission inventories cannot be expected to yield close hour-to-hour correspondences. This would need careful modeling of the actual flow field at each receptor site, and the use of a very fine emission inventory with individual source heights. Fig. 7, however, shows that there is neither a general underprediction nor overprediction during certain hours of the day: the nighttime concentration level is predicted well, and the height of the concentration peaks during daytime always is of similar magnitude. This result is due to the combined effect of the storage term in the urban energy balance (Eq. 5) and the lower limit to the absolute value of the Obukhov length (Eq. 7).

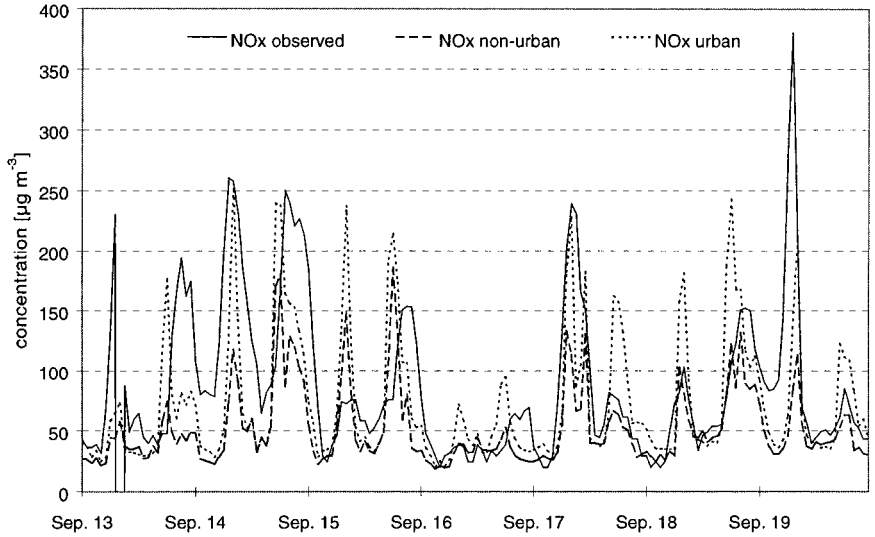

FIG. 7. Example of hourly concentration data for NO_x for the "Kaserne" location. The measured concentration (hourly averages) as well as OML model predictions with an urban and a traditional nonurban setup are depicted.

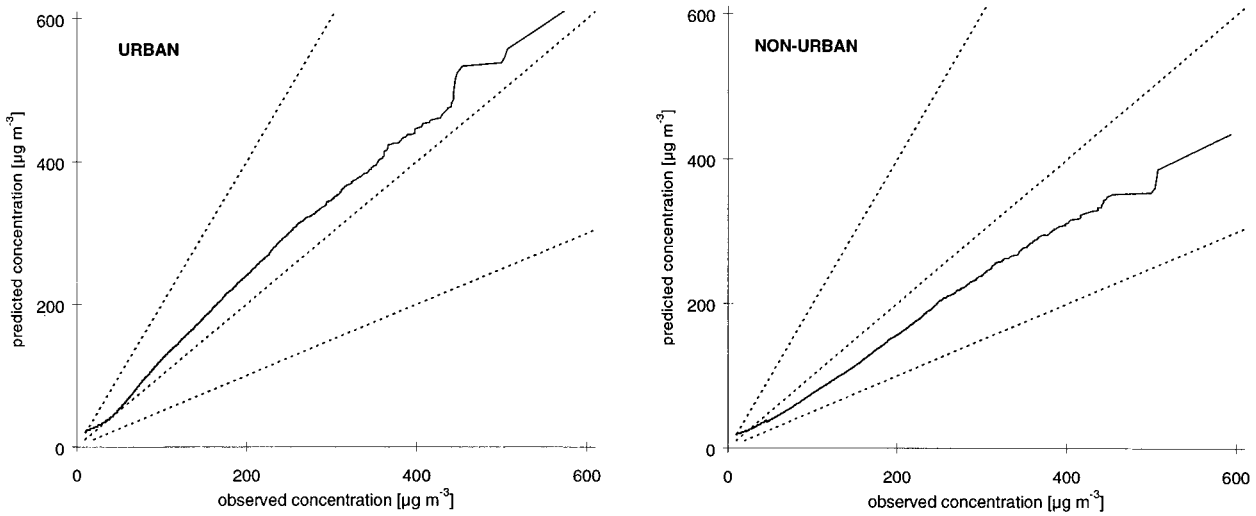

FIG. 8. Quantile–quantile plot of hourly NO_x concentrations at the Kaserne location for urban and nonurban model simulations. The upper and lower dashed lines indicate the range of predictions within a factor of 2 of observations.

Figure 8 depicts the so-called quantile–quantile plot for one of the four stations with continuous measurements. For both the urban and nonurban setup, the graph is almost a straight line, indicating that the frequency distribution of predicted low and high concentrations corresponds very well to observations. The urban simulation leads to a general increase of predicted concentrations of 37%.

e. Annual averages: Statistical performance

A scatterplot with the annual averaged NO_x and SO_2 concentrations is depicted in Fig. 9. The different monitoring site groups Q1 to Q3 are marked with different symbols; in addition, large symbols denote stations with continuous measurements. For all stations, both the urban and nonurban simulation results are shown (filled and open symbols, respectively). In Table 7, the following statistical measures are compared for the two different simulations:

FB	the fractional bias: $FB = (\overline{C}_{obs} - \overline{C}_{pred})/[0.5(\overline{C}_{obs} + \overline{C}_{pred})]$,
NMSE	the normalized mean-square error: $NMSE = \overline{(C_{obs} - C_{pred})^2}/(\overline{C}_{obs}\overline{C}_{pred})$,
COR	the correlation coefficient: $COR = \overline{(C_{obs} - \overline{C}_{obs})(C_{pred} - \overline{C}_{pred})}/(\sigma_{obs}\sigma_{pred})$, and
FAC2	percentage of simulations within a factor of 2 of the measurement.

Here, C_{obs} is the observed concentration and C_{pred} is the predicted one.

The performance of the OML-Urban model, with FAC2 = 100% for NO_x and SO_2 for Q1 and Q2 stations, is considered to be very satisfactory, showing that Gaussian plume models may be applied to urban environments (when some corrections are made) for the prediction of yearly averaged concentration. For hourly averaged concentrations, of course, the variability is much larger. As expected (section 3b), the model performance is best for Q1 monitoring stations and is second best for Q2 data, whereas, for Q3 locations, the local influence of major roads (not fully resolved by the gridded emission inventory) causes a slight underprediction of ground-level concentrations.

The bootstrap resampling method proposed by Hanna (1989) has been used to assess whether there are systematic errors at the 95% confidence level. The NO_x predictions are almost bias free, the FB values of 0.051 and 0.038 for Q1 and Q2 sites, respectively, not being significantly different from zero. Also, the FB value, of -0.037, for Q1 stations for SO_2 does not differ significantly from zero, but it does for Q2 data. Figure 9 also confirms that, whereas for NO_x the urban approach leads to an essentially bias-free prediction, for SO_2 the underprediction for the nonurban approach turns into a slight overprediction when using the urban setup. Especially, the annual-average concentration observed at the two continuously measuring stations being classified as Q1 or Q2 is very closely reproduced for NO_x. For SO_2, a small systematic overprediction of concentrations persists.

Table 8 gives the relationship between 1) the proportions of domestic/industrial and traffic area source emissions, and 2) the contributions of the respective source categories to the predicted ground-level (at the lower model boundary, i.e., $z = 9$ m) concentration. The combined effect of the higher emission height and the more pronounced buoyancy of the domestic/industrial emissions causes a decrease in the contribution to the concentration impact, as compared with the share in the emissions. For example, although over 38% of all NO_x emissions originate from nonmobile sources, the street-level concentrations (when the arithmetic

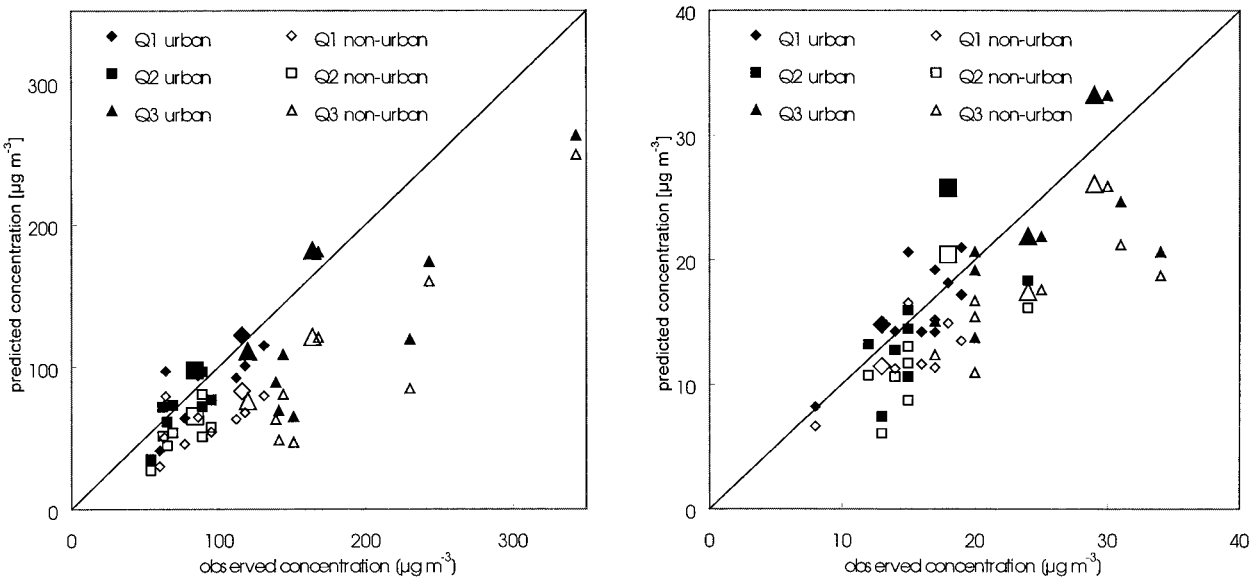

FIG. 9. Scatterplot of yearly average concentration for (left) NO_x and (right) SO_2 for 1990. Model predictions are depicted for urban and nonurban model simulations. Enlarged symbols mark those stations for which continuous (hourly) measurement data are available.

mean over all station locations is computed) are influenced by the traffic emissions by almost 84% (without the background concentration).

5. Summary and conclusions

To obtain a proper modification of operational (Gaussian) dispersion models for use within an urban environment, the concept of an ''urban preprocessor'' (Rotach 1997a) has been introduced. Its basic principle is to use similarity theory based on local fluxes for the parameterization of the turbulence structure within the urban roughness sublayer. The first validation step of this concept has been reported on elsewhere (Rotach and de Haan 1997) and was performed by use of a Lagrangian particle dispersion model for the simulation of a (sub)urban tracer experiment. A clear improvement of the model performance was the result. This result indicates that the urban preprocessor is able to take into account better the rough character of the surface at the sites where this experiment took place. As a second validation step, the performance of the operational Gaussian multisource dispersion model OML for this experiment (Copenhagen) and for Lillestrøm showed a similar improvement of the correspondence between the simulated and the measured concentrations when the roughness sublayer is introduced (de Haan et al. 1998). Therefore, the concept of the urban preprocessor can be used with operational Gaussian dispersion models to improve the models' prediction skills over urban surfaces.

The resulting OML-Urban model is used for the case study of the yearly average surface pollution concentration (NO_x and SO_2) in the city of Zurich in 1990, for which a very detailed emission inventory (100 m $\times$ 100 m resolution) is available. Some parameterizations within OML's meteorological preprocessor were changed in accordance with an urban energy budget. Data from air pollution monitoring stations were grouped according to the influence of nearby roads. The performance of OML-Urban is assessed for these different groups separately. The resulting prediction skill is very satisfactory, with a close reproduction of the frequency distribution of observed concentration, all predictions being within a factor of 2 of the observed values and having

TABLE 7. Model prediction performance for urban and nonurban model setup and meteorological preprocessor. For definition of FB, NMSE, COR, FAC2 see text.

Approach	Station group	NMSE	FB	COR	FAC2
Observations		0.000	0.000	1.000	100%
NO_x					
Urban	All	0.132	0.178	0.845	93%
	Q1	0.038	0.051	0.749	100%
	Q2	0.031	0.038	0.732	100%
	Q3	0.161	0.300	0.781	80%
Nonurban	All	0.355	0.465	0.870	82%
	Q1	0.229	0.395	0.616	90%
	Q2	0.145	0.338	0.728	100%
	Q3	0.372	0.548	0.884	60%
SO_2					
Urban	All	0.053	0.053	0.770	100%
	Q1	0.023	−0.037	0.774	100%
	Q2	0.079	0.061	0.592	100%
	Q3	0.054	0.108	0.657	100%
Nonurban	All	0.113	0.260	0.821	96%
	Q1	0.055	0.184	0.779	100%
	Q2	0.119	0.256	0.669	88%
	Q3	0.128	0.311	0.759	100%

TABLE 8. Contribution of different source categories to the total emission and predicted surface concentrations (arithmetic mean over all station locations, without the background concentration).

	Share in annual emission				Contribution to surface concentration			
	SO_2		NO_x		SO_2		NO_x	
Source category	(t yr^{-1})	(%)	(t yr^{-1})	(%)	($\mu g\ m^{-3}$)	(%)	($\mu g\ m^{-3}$)	(%)
Heating/industrial	1905	93.5%	1960	38.1%	13.8	81.0%	13.3	16.2%
Traffic	132	6.5%	3189	61.9%	3.2	19.0%	68.5	83.8%
Sum	2037	100.0%	5149	100.0%	17.0	100.0%	81.8	100.0%

a small systematic error (bias). It is concluded that the method presented is suitable to allow the application of Gaussian plume models to urban environments for the prediction of yearly averaged concentrations.

Acknowledgments. The comments and suggestions of Dr. S. R. Hanna, Dr. H. R. Olesen, and P. Løfstrøm have been very helpful. The comments of the three anonymous reviewers further improved the manuscript. Thanks go to Dr. J. Heldstab and Dr. T. Künzle for providing the background NO_x concentration map for Zurich. The work was partly financed by the Swiss Agency of Education and Sciences (BBW) through the TMR network (TRAPOS) and by the Swiss National Science Foundation through Grant 21-46849.96.

REFERENCES

Arnfield, A. J., and C. S. B. Grimmond, 1998: An urban canyon energy budget model and its application to urban heat flux modeling. *Energy Build.,* **27,** 61–68.

Berkowicz, R., and L. P. Prahm, 1982: Sensible heat flux estimated from routine meteorological data by the resistance method. *J. Appl. Meteor.,* **21,** 1845–1864.

——, H. R. Olesen, and U. Torp, 1985: The Danish Gaussian air pollution model (OML): Description, test and sensitivity analysis in view of regulatory applications. *Air Pollution Modeling and its Applications V,* C. De Wispelaere, F. A. Schiermeyer, and N. V. Gillani, Eds., Plenum Press, 453–481.

Briggs, G. A., 1984: Plume rise and buoyancy effects. *Atmospheric Science and Power Production,* D. Randerson, Ed., DOE/TIC 27601, Department of Commerce, 327–366.

Buck, A., 1981: New equations for computing vapor pressure and enhancement factor. *J. Appl. Meteor.,* **20,** 1527–1532.

Carruthers, D. J., and Coauthors, 1992: UK Atmospheric Dispersion Modelling System. *Air Pollution Modelling and its Applications IX,* H. van Dop and G. Kallos, Eds., Plenum Press, 15–28.

de Haan, P., M. W. Rotach, and M. Werfeli, 1998: Extension of an operational short-range dispersion model for applications in an urban environment. *Int. J. Veh. Des.,* **20,** 105–114.

Feigenwinter, C., R. Vogt, and E. Parlow, 1999: Vertical structure of selected turbulence characteristics above an urban canopy. *Theor. Appl. Climatol.,* **62,** 51–63.

Gryning, S.-E., and E. Lyck, 1984: Atmospheric dispersion from elevated sources in an urban area: Comparisons between tracer experiments and model calculations. *J. Climate Appl. Meteor.,* **23,** 651–660.

Hanna, S. R., 1989: Confidence limits for air quality model evaluations, as estimated by bootstrap and jackknife resampling methods. *Atmos. Environ.,* **23,** 1385–1398.

——, and J. C. Chang, 1992: Applied dispersion modeling over urban areas. *Bound.-Layer Meteor.,* **58,** 229–259.

——, and ——, 1993: Hybrid Plume Dispersion Model (HPDM) improvements and testing at three field sites. *Atmos. Environ.,* **27A,** 1491–1508.

Härkönen, J., J. Kukkonen, E. Valkonen, and A. Karppinen, 1998: The influence of vehicle emission characteristics and meteorological conditions on urban NO_2 concentrations. *Int. J. Veh. Des.,* **20,** 125–130.

Högström, U., H. Bergström, and H. Alexandersson, 1982: Turbulence characteristics in a near-neutrally stratified urban atmosphere. *Bound.-Layer Meteor.,* **23,** 449–472.

Holtslag, A. A. M., and A. P. van Ulden, 1983: A simple scheme for daytime estimates of the surface fluxes from routine weather data. *J. Climate Appl. Meteor.,* **22,** 517–529.

Lee, I. Y., and H. M. Park, 1994: Parametrization of the pollutant transport and dispersion in urban street canyons. *Atmos. Environ.,* **28,** 2324–2349.

Monteith, J. L., 1981: Evaporation and surface temperature. *Quart. J. Roy. Meteor. Soc.,* **107,** 1–27.

Nielsen, L. B, L. P. Prahm, R. Berkowicz, and K. Conradsen, 1981: Net incoming radiation estimated from hourly global radiation and/or cloud observations. *J. Climatol.,* **1,** 255–272.

Oikawa, S., and Y. Meng, 1995: Turbulence characteristics and organized motion in a suburban roughness sublayer. *Bound.-Layer Meteor.,* **74,** 289–312.

Oke, T. R., 1988: The urban energy balance. *Progr. Phys. Geogr.,* **12,** 471–508.

——, and H. A. Cleugh, 1987: Urban heat storage derived as energy balance residuals. *Bound.-Layer Meteor.,* **39,** 233–245.

Olesen, H. R., 1995: The model validation exercise at Mol: Overview of results. *Int. J. Environ. Pollut.,* **5,** 761–784.

——, and N. Brown, 1992: The OML meteorological preprocessor; a software package for the preparation of meteorological data for dispersion models. MST Luft-A 122, 2d ed. [Available from National Environmental Research Institute, DK-4000 Roskilde, Denmark.]

——, P. Løfstrøm, R. Berkowicz, and A. B. Jensen, 1992: An improved dispersion model for regulatory use: The OML model. *Air Pollution Modeling and its Applications IX,* H. van Dop and G. Kallos G., Eds., Plenum Press, 29–38.

Rafailidis, S., 1997: Influence of building areal density and roof shape on the wind characteristics above a town. *Bound.-Layer Meteor.,* **85,** 255–271.

Raupach, M. R., R. A. Antonia, and S. Rajagopalan, 1991: Rough-wall turbulent boundary layers. *Appl. Mech. Rev.,* **44,** 1–25.

Rotach, M. W., 1993a: Turbulence close to a rough urban surface. Part I: Reynolds stress. *Bound.-Layer Meteor.,* **65,** 1–28.

——, 1993b: Turbulence close to a rough urban surface. Part II: Variances and gradients. *Bound.-Layer Meteor.,* **66,** 75–92.

——, 1994: Determination of the zero plane displacement in an urban environment. *Bound.-Layer Meteor.,* **67,** 187–193.

——, 1997a: Towards meteorological preprocessing for dispersion models in an urban environment. *Int. J. Environ. Pollut.,* **8,** 548–556.

——, 1997b: The turbulence structure in an urban roughness sublayer. *Flow and Dispersion through Groups of Obstacles,* R. J. Perkins and S. E. Belcher, Eds., Clarendon Press, 143–155.

——, 2001: Simulation of urban-scale dispersion using a Lagrangian stochastic dispersion model. *Bound-Layer Meteor.,* in press.

——, and P. de Haan, 1997: On the urban aspect of the Copenhagen data set. *Int. J. Environ. Pollut.,* **8,** 279–286.
——, S.-E. Gryning, and C. Tassone, 1996: A two-dimensional stochastic Lagrangian dispersion model for daytime conditions. *Quart. J. Roy. Meteor. Soc.,* **122,** 367–389.
Roth, M., 1993: Turbulent transfer relationships over an urban surface. II: Integral statistics. *Quart. J. Roy. Meteor. Soc.,* **119,** 1105–1120.
——, 2000: Review of atmospheric turbulence over cities. *Quart. J. Roy. Meteor. Soc.,* **126,** 941–990.
——, and T. R. Oke, 1993: Turbulent transfer relationships over an urban surface. I: Spectral characteristics. *Quart. J. Roy. Meteor. Soc.,* **119,** 1071–1104.
SAEFL, 1997: NO_2 concentration in Switzerland 1990 to 2010 (in German or French, with English abstract). SRU No. 289, 58 pp. [Available from Swiss Agency for Environment, Forests and Landscape (SAEFL), 3003 Berne, Switzerland.]
Stull, R. B., 1988: *An Introduction to Boundary Layer Meteorology.* Kluwer Academic Publishers, 666 pp.
Werfeli, M., 1995: Modelling surface pollutant concentrations (SO2 and NOx) in the city of Zurich. *Int. J. Environ. Pollut.,* **5,** 575–584.
Zoumakis, N. M., 1995: A note on average vertical profiles of vehicular pollutant concentrations in urban street canyons. *Atmos. Environ.,* **29,** 3719–3725.